ChemComm

Accepted Manuscript

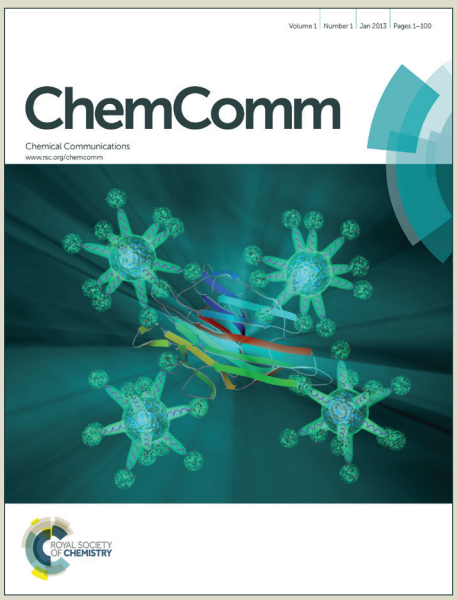

ROYAL SOCIETY OF CHEMISTRY

www.rsc.org/chemcomm

Journal Name

RSCPublishing

COMMUNICATION

Self Reduction of Copper Complex MOD Ink for Inkjet Printing Conductive Patterns on Plastics

Cite this: DOI: 10.1039/xoxxoooooox

Yousef Farraj, Michael Grouchko, and Shlomo Magdassi*

Received ooth January 2012,
Accepted ooth January 2012

DOI: 10.1039/xoxxoooooox

www.rsc.org/

Highly conductive copper patterns on low-cost flexible substrates are obtained by inkjet printing a metal complex based ink. Upon heating the ink, the soluble complex, which is composed of copper formate and 2-amino-2-methyl-1-propanol, decomposes under nitrogen at 140°C and is converted to pure metallic copper. The decomposition process of the complex is investigated and a suggested mechanism is presented. The ink is stable in air for prolonged periods, with no sedimentation or oxidation problems, which are usually encountered in copper nanoparticle based inks.

The field of printing conductive contacts by metallic inks has been gaining great interest, due to its importance for printed electronics.[1] Usually, two main types of ink are being used, metal nanoparticle-based ink, and a metal organic decomposition (MOD) ink.[2] Due to its low resistivity (1.59 μΩ·cm) and high stability, silver is the most commonly used metal. However, the high cost of silver-based inks pose a high barrier for a large-scale use in the production of low-cost plastic electronic devices. Therefore, there is an unmet need for inks with low-cost high conductive metals. The best candidate is copper, with the second lowest resistivity (1.72 μΩ·cm) and a significantly lower cost, compared to silver (factor of ~90). A major challenge in inks containing copper nanoparticles is the very rapid oxidation rate in air, during storage and during the sintering step, which is essential in obtaining conductive percolation paths.[3] MOD copper[4] ink enables to overcome the oxidation of copper during storage, since the metal is already present in its oxidized form. To date, to our best knowledge, none of the reported studies have focused on the investigation of the complex decomposition mechanism. In addition, so far all the reported MOD copper inks contain volatile solvents (e.g. alcohols, amines, water, toluene, etc.) which limit their use in inkjet printing due to their high evaporation rate.

Here we present an MOD ink, capable of self reduction upon its decomposition at low temperature. The ink contains hydrous copper formate (CuFormate×2H2O) complexed with 2-amino-2-methyl-1-propanol (CuF-AMP), which undergoes pyrolysis to generate copper metallic patterns at low temperatures, thus enabling the printing of conductors on heat sensitive plastic substrates such as PET (poly ethylene terephthalate) and PEN (poly ethylene naphthalate).[4e, 5] The ink is chemically stable, and is composed of a low viscosity solution of the complex, making it suitable for inkjet printing. After printing, heating to 140 °C enables direct formation of large and connected copper grains.

As presented below, the CuF-AMP decomposition process leads to the formation of a copper metal, due to the reducing counter ion in the complex (formate). This enables the conversion process to be carried under nitrogen gas only, thus overcoming the need to perform the process under reducing atmosphere such as hydrogen gas [4b, 4d, 4f] or formic acid vapors.[4a, 4f]

The advantages of the formate counter ion are: (i) low organic content of the complex, and therefore inks with high copper load can be prepared, (ii) the decomposition products are volatile, thus there are no undesired residues in the printed pattern that can lead to low conductivity, and (iii) the low decomposition temperature enables printing at low cost, temperature sensitive plastic substrates. Furthermore, as suggested in Eq. 1, the self reduction reaction by the formate is also accompanied by the release of hydrogen gas that may further contribute to the reducing atmosphere, thus assisting in preventing oxidation of the formed copper.

$$(1)\ Cu(HCOO)_2 \xrightarrow{\Delta} Cu_{(s)} + H_{2(g)}\uparrow + 2CO_{2(g)}\uparrow$$

$$Cu^{2+} + 2e^- \rightarrow Cu_{(s)}$$

$$2HCOO^- \rightarrow 2CO_{2(g)} + H_{2(g)} + 2e^-$$

As indicated previously by Galwey et al.[6] the decomposition mechanism of copper formate takes place in two stages. In the first stage, the divalent copper ion is partially reduced to monovalent copper ion and only then the copper ion is fully reduced (Eq. 2):[6-7]

$$(2)\ Cu^{II}(HCOO)_2 \rightarrow Cu^{I}(HCOO) + CO_{2(g)} + \frac{1}{2}H_{2(g)}$$

$$Cu^{I}(HCOO) \rightarrow Cu_{(s)} + CO_{2(g)} + \frac{1}{2}H_{2(g)}$$

As suggested in our previous publication[5] and by Shin et al.,[4c] copper complexes of amino-hydroxyl compounds are advantageous, due to their high stability during processing and storage, and since the decomposition of most of them occurs at sufficiently low temperatures (lower than the decomposition temperature of the metal salt and low enough to enable the use of plastic substrates). Furthermore, amino hydroxyl compounds enable good solubility of the copper complexes in glycol ether solvents, which are very suitable for inkjet printing (low viscosity, surface tension, and evaporation rates). We, therefore, evaluated the following amino hydroxyl compounds as the complexing ligands: diisopropanolamine, ethanolamine, 3-amino-1-propanol, diethanolamine, 1-amino-2-propanol, and 2-amino-2-methyl-1-propanol (AMP). With all these amino-hydroxyl compounds, deep-blue to purple complexes were obtained.

According to the Hard Soft Acid Base theory (HSAB), a bidentate binding of the amino-hydroxyl compound is possible. This was confirmed by Nieuwpoort et al. who stated that amino hydroxyl compounds are randomly connected to the metals, either by a bidentate bond (see Fig. S1 in ESI) or as a monodentate ligand[8] through the nitrogen group. In that case, some of the hydroxyl groups are free to form hydrogen bonds with the glycols ether solvent and, therefore, to enhance the complex solubility in such solvents. That assortment of ligand binding, would increase the number of different structures to be generated, e.g. multinuclear complexes, in various copper oxidation states (monovalent and divalent).[9]

Since the final goal of this work is to print conductive patterns, the effect of the ligand on the obtained conductivity was evaluated. Therefore, various copper formate-ligand complexes were formed by mixing the copper salt with various ligands, at a constant molar ratio of 1:2, respectively. It was found that the presence of these ligands clearly affects the decomposition temperature of the copper formate, while the AMP ligand leads to both, a decrease in the decomposition temperature and the achievement of the best conductivity. The main difference between AMP and the other ligands is the presence of a tertiary carbon. Shin et al[4c] suggested that this tertiary carbon contributes to the formation of small volatile by-products, unlike other amino hydroxyl ligands, which enable polymerization reactions between the carbon dioxide and other organic by-products.[10]

Figure 1 presents the differential scanning calorimetry (DSC) and thermo gravimetric analysis (TGA) plots of the copper formate salt ink and copper formate-AMP complex ink.[4e] It can be clearly seen that: (i) the complex has a significantly lower decomposition temperature, compared to the copper formate (150 °C vs. 200 °C), (ii) The copper formate decomposition is accompanied by a small exothermic peak, a one step process, while the copper formate-AMP complex decomposition takes place in two stages. A clear exothermic peak is followed by a large endothermic peak. XRD analyses of the resulting materials in both cases indicate the formation of pure crystalline fcc copper (Fig. S2 in ESI). It should be noted that the difference in the percentage of the remaining copper in the salt and in the complex, (43% and 26%), reflects the theoretical content of the copper in each (41.4% and 26.1%).

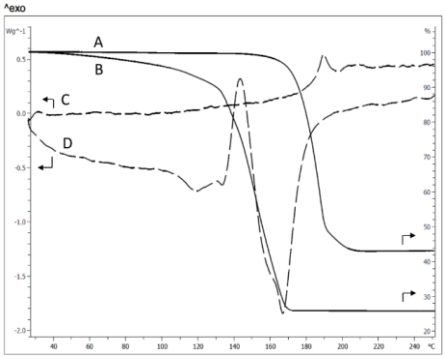

Fig. 1: DSC-TGA plots of copper salt (A and C) and copper complex (B and D).

In order to better understand the reason for the decrease in the decomposition temperature, the dihydrated copper salt and the complex were characterized by simultaneous thermal analysis, coupled with mass spectrometry (STA-MS). Figure 2A presents the DSC-TGA results of the hydrated copper salt. It can be seen that the mass loss takes place in two steps: the first is between 70–100 °C and the second, between 180-200 °C. These two mass losses can be attributed first to the water evaporation (endothermic peak in DSC), followed by a drastic mass loss due to the release of CO_2, accompanied by the decomposition of the copper salt and generation of pure metallic copper (small exothermic peak in Fig. 2A). Furthermore, it was found that the first weight loss due to evaporation of water correlates well with the expected weight loss due to the dehydration of the salt (18.3% vs. 19%). These TGA-DSC results correlate well with the STA-MS results presented in Figure 2B, which show that the main two gaseous products of the hydrated copper formate decomposition are CO_2 and H_2O. In contrast, in the case of the complex (description of the complex formation in ESI), the decomposition process takes place at a much lower temperature, showing many more gaseous by-products. Figure 2D presents the main gaseous by-products and their release as a function of temperature. These TGA-DSC and MS results indicate the following: (i) The water evaporates in two processes, the first for the non-bound water (peak at 110°C) and the second for the bound water (peak at 185 °C), (ii) The decomposition takes place in two steps, first at 150 °C, accompanied by the release of CO_2 and carbon, and then at 185 °C, with the release of CO_2, H_2O and various fragments of AMP, (iii) The first CO_2 release is accompanied by an exothermic DSC peak, while the second CO_2 release is accompanied by an endothermic peak.

Therefore, these results correlate well with Eq. (2). In the first stage copper (II) is reduced to copper (I), when the first formate ion is released as CO_2 (exothermic peak in DSC). Then, copper (I) is further reduced to metallic copper and the second formate is released as CO_2 (endothermic peak in DSC due to crystallization of copper) (see Figure S3 of XPS analysis in ESI).

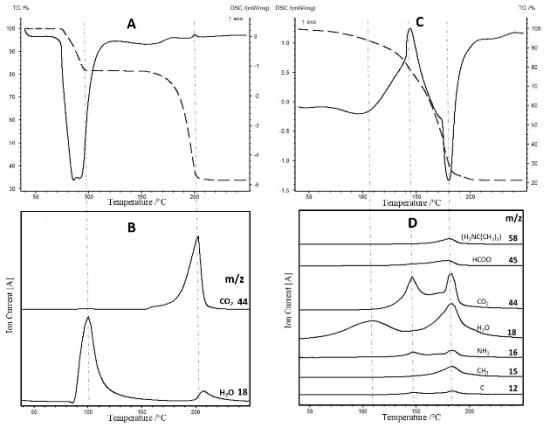

Fig. 2: DSC/TGA-MS of the copper formate salt (A+B) dihydrate and (C+D) copper formate dihydrate complex. The mass to charge ratio (m/z) detected as products of pyrolysis were related to carbon (amu=12), methyl (amu=15), amidogen (amu=16), water (amu=18), carbon dioxide (amu=44), formate (amu=45), and fragment of AMP (amu=58).

The DSC-MS results (Fig. 2B and 2D) not only reveal the two-step mechanism mentioned above, but also the fact that the second decomposition step is accompanied by the release of H_2O. The proposed decomposition is presented in scheme 1.

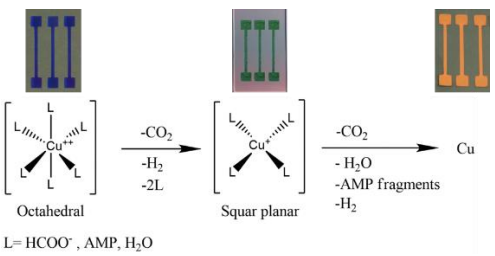

Scheme 1: A suggested mechanism for the decomposition of the complex from octahedral to square planar configuration to metallic copper. An image of the obtained film at each stage is presented on top.

The role of the water molecules in the complex structure and decomposition process was further studied by using anhydrous copper formate to form the complex. The MS plot (Fig. 3) reveals a clear difference between the gaseous by-products of the anhydrous complex and the hydrated complex (Fig. 2D). First, the peaks of the gaseous by-products of the anhydrous CuF-AMP complex are much weaker in relation to the hydrated copper formate complex, and the CO_2 is the only significant gaseous by-product. Obviously, these non-volatile by-products should have a clear effect on the obtained copper film and, as presented below, may explain the difference in the resistivity values between the hydrated and non-hydrated complexes. Second, no peak of coordinated water was observed for the hydrated complex (the unexpected peak of water between 90°C to 120°C can be attributed to insufficient dry reagents). The absence of a water peak at 180°C provides a clear proof that the water peak at 180°C in Figure 2D (for the hydrated complex) belongs to coordinated water and not to an *in situ* water formation within the decomposition process (as suggested in Eq. 3).[11]

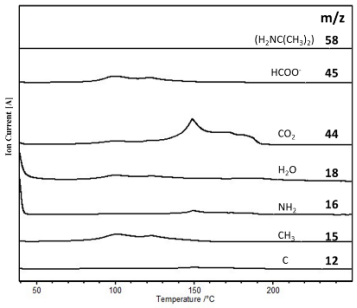

Fig. 3: MS curve for decomposition of anhydrated copper complex at heating rate 10 °C/min under nitrogen atmosphere.

$$(3)\ Cu(HCOO)_2 \rightarrow Cu_{(s)} + H_2O_{(g)} + CO_{(g)} + CO_{2(g)}$$

Therefore, as suggested in Scheme 2, the water in the complex may participate in the decomposition process in two ways: a. by being responsible for catalyzing the formate decomposition (Scheme 2A),[12] and b. by acting as an acid that causes the disconnection of the basic ligand, AMP, (Scheme 2B).[13] The latter may also increase the lability of the complex, which demonstrates how easily metal-ligand bonds are broken and disengaged.

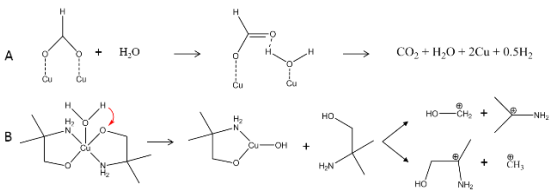

Scheme 2: Water effect on system: (A) Formate decomposition catalyzed by water, (B) Ligand disconnecting due to existence of water.

All these results demonstrate that the uniqueness of this hydrated CuF-AMP complex is dual: (i) the decreased decomposition temperature of copper formate, and (ii) the complete decomposition of the organic content (formate and AMP) which leads to its release as gaseous by-products. As presented below, the last point is critical in order to achieve high conductivity of the printed patterns.

In order to obtain conductive layers, the solutions of hydrated CuF-AMP and anhydrous CuF-AMP complexes were placed by draw-down (18 µm wet film thickness) on a glass slide. Then it was preheated in air at 130 °C for 7 minutes (till the complex color turned from blue to green), and then heated at various temperatures (140 to 250 °C, see Fig. 4A) under nitrogen flow for 2 minutes. It was expected that the anhydrous complex, which contained 13% more copper, would lead to a lower resistivity compared to the hydrated complex. However, it was found that the hydrated complex led to a four time lower resistivity compared to the anhydrous complex. This can be explained by the above suggested mechanism, in which the unique role of water in the decomposition of the complex, was revealed. Furthermore, the MS results presented in Figures 2D and 3 indicate that organic by-products in the anhydrous complex (for example, carbon dioxide and AMP) are weak in relation to that of the hydrated complex. Probably, polymerization reactions carried out between CO_2 and AMP that led to the formation of non-volatile organic residues, impeded the development of sufficiently connected

particles and, thereby, increased the resistivity.[10] Therefore, our results indicate that water molecules, which enable the complete decomposition of the complex, lead to copper films with less organic residues, accompanied by many more percolation paths and thus to higher conductivity.

Figure 4A presents the obtained sheet resistance of films of the hydrated complex as a function of temperature. As shown, the lowest sheet resistance was obtained at 190 °C, less than 0.1 Ohms/square (10.5 μΩ*cm). For comparison, under the same conditions, the anhydrous complex led to 45 μΩ*cm. SEM micrographs, presents the effect of the decomposition temperature on the obtained copper films morphology. It can be seen that as the temperature increases, the grain size decreases. Still, it seems that the best contact between the particles is obtained at 190 °C. This phenomenon may be explained by means of nucleation *vs*. sintering. On the one hand, particle size decreases as the decomposition temperature goes up, due to the formation of more nuclei caused by more rapid decomposition. On the other hand, as the particle size decreases, the number of junctions between the particles grow, causing the sheet resistance to increase. Yet, it is well known that the sintering between the particles increases as the temperature increases.[14] It seems that the optimum of these two contradicting processes is obtained at a moderate temperature of 190 °C, while enabling the formation of large enough particles, and yet enable their sintering.

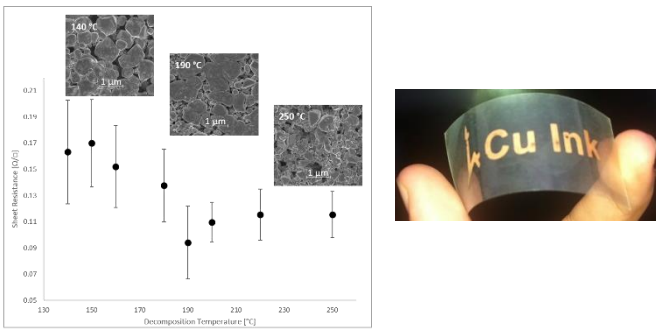

Fig. 4: (A) Plot of sheet resistance vs. decomposition temperature with SEM micrographs at various temperatures. (B) Ink-Jet printed copper patterns on PET film while using the copper complex ink.

Based on these findings, the solution of the hydrated AMP complex was inkjet printed while using OmniJet100 (UniJet) equipped with Dimatix DMC (10pl) heads. Various patterns could be printed on glass, PET and PEN. Figure 4B presents an example of a conductive copper pattern inkjet printed on PEN.

In Conclusion, the advantages of the copper MOD inks described above are the ability to undergo self- reduction, they are chemically stable, has a lower decomposition temperature as compared to the copper salt, they are easy to process in inkjet printing, and their preparation is very simple and feasible. Two main issues were investigated in this study. First, we prepared a copper complex based ink which is very suitable for inkjet printing of conductive patterns on plastics, due to its low decomposition temperature, yielding resistivity of 10.5 μΩ*cm (conductivity of about 16% of bulk copper). Second, we revealed the complex decomposition mechanism, while finding the important role of water for obtaining highly conductive patterns at low temperatures. Finally, successfully printed copper patterns were obtained on transparent flexible substrates as PET and PEN.

Notes and references

Casali Center for Applied Chemistry, Institute of Chemistry, The Center for Nanoscience and Nanotechnology, The Hebrew University of Jerusalem, Edmond J. Safra Campus, Givat Ram, Jerusalem, 91904, Israel
E-mail: magdassi@mail.huji.ac.il;

1(a) J. Perelaer, P. J. Smith, D. Mager, D. Soltman, S. K. Volkman, V. Subramanian, J. G. Korvink and U. S. Schubert, *Journal of Materials Chemistry*, 2010, **20**, 8446; (b) A. Kamyshny, J. Steinke and S. Magdassi, *Open Applied Physics Journal*, 2011, **4**, 19.
2(a) S. B. Walker and J. A. Lewis, *Journal of the American Chemical Society*, 2012, **134**, 1419; (b) X. Nie, H. Wang and J. Zou, *Applied Surface Science*, 2012, **261**, 554; (c) D. Kim, S. Jeong, S. Lee, B. K. Park and J. Moon, *Thin Solid Films*, 2007, **515**, 7692; (d) M. Grouchko, A. Kamyshny and S. Magdassi, *Journal of Materials Chemistry*, 2009, **19**, 3057.
3 S. Magdassi, M. Grouchko and A. Kamyshny, *Materials*, 2010, **3**, 4626.
4(a) S. J. Kim, J. Lee, Y.-H. Choi, D.-H. Yeon and Y. Byun, *Thin Solid Films*, 2012, **520**, 2731; (b) Y.-I. Lee, K.-J. Lee, Y.-S. Goo, N.-W. Kim, Y. Byun, J.-D. Kim, B. Yoo and Y.-H. Choa, *Japanese Journal of Applied Physics*, 2010, **49**, 086501; (c) D.-H. Shin, S. Woo, H. Yem, M. Cha, S. Cho, M. Kang, S. Jeong, Y. Kim, K. Kang and Y. Piao, *ACS applied materials & interfaces*, 2014, **6**, 3312; (d) B. Lee, Y. Kim, S. Yang, I. Jeong and J. Moon, *Current Applied Physics*, 2009, **9**, e157; (e) *US Pat., WO2010109465 (A1), 2010*; (f) Y.-H. Choi, J. Lee, S. J. Kim, D.-H. Yeon and Y. Byun, *Journal of Materials Chemistry*, 2012, **22**, 3624; (g) D. Adner, M. Korb, S. Schulze, M. Hietschold and H. Lang, *Chemical Communications*, 2013, **49**, 6855.
5 *US Pat., WO2013128449 (A2), 2013*.
6 A. K. Galwey, D. Jamieson and M. E. Brown, *The Journal of Physical Chemistry*, 1974, **78**, 2664.
7(a) M. A. Mohamed, A. K. Galwey and S. A. Halawy, *Thermochimica acta*, 2004, **411**, 13; (b) B. Lee, S. Jeong, Y. Kim, I. Jeong, K. Woo and J. Moon, *Metals and Materials International*, 2012, **18**, 493; (c) A. A. Vecher, S. V. Dalidovich and E. A. Gusev, *Thermochimica Acta*, 1985, **89**, 383.
8 G. Nieuwpoort and W. Groeneveld, *Recueil des Travaux Chimiques des Pays-Bas*, 1980, **99**, 394.
9(a) H. Muhonen and R. Hämäläinen, *Acta Chemica Scandinavica*, 1978, **32A**, 5; (b) J. Bertrand, E. Fujita and D. VanDerveer, *Inorganic Chemistry*, 1980, **19**, 2022; (c) H. Muhonen, *Acta Crystallographica Section B: Structural Crystallography and Crystal Chemistry*, 1981, **37**, 951; (d) *Acta Crystallographica Section B: Structural Crystallography and Crystal Chemistry*, 1982, **38**, 2041; (e) *Acta Crystallographica Section C: Crystal Structure Communications*, 1983, **39**, 536; (f) H. Muhonen and W. E. Hatfield, *Acta Chemica Scandinavica*, 1986, **40A**, 11; (g) H. Muhonen, W. E. Hatfield and J. H. Helms, *Inorganic Chemistry*, 1986, **25**, 800; (h) H. Muhonen, *Inorganic Chemistry*, 1986, **25**, 4692.
10(a) C. Gouedard, D. Picq, F. Launay and P.-L. Carrette, *International Journal of Greenhouse Gas Control*, 2012, **10**, 244; (b) H. Lepaumier, D. Picq and P.-L. Carrette, *Industrial & Engineering Chemistry Research*, 2009, **48**, 9061.
11 A. Keller and F. Korosy, *Nature*, 1948, **162**, 580.
12 K. L. Miller, C. W. Lee, J. L. Falconer and J. W. Medlin, *Journal of Catalysis*, 2010, **275**, 294.
13 M. BuFaroosha, Michigan State University, 2002.
14 K. K. Nanda, *Pramana - J Phys*, 2009, **72**, 617.